Eur. Phys. J. B **50**, 631–637 (2006)
DOI: 10.1140/epjb/e2006-00168-y

THE EUROPEAN PHYSICAL JOURNAL B

Numerical studies of gravity destabilized percolation in 2D porous media

Z. Bo[1,2], D. Loggia[1,a], L. Xiaorong[1], G. Vasseur[3], and H. Ping[1]

[1] Key Laboratory of Mineral Resource, Institute of Geology and Geophysics, Chinese Academy of Sciences, Beijing 100029, P.R. China
[2] Laboratoire de tectonophysique (UMR5568), ISTEEM, CNRS & Université Montpellier II, 34095 Montpellier, France
[3] SISYPHE, UMR, Boîte 123, Université Paris 6, 75252 Paris Cedex 05, France

Received 22 April 2005 / Received in final form 3 January 2006
Published online 17 May 2006 –

Abstract. Two dimensional simulations of percolation are realized on square networks of pore throats with a random capillary pressure distribution. We analyse the influence of a destabilizing gravity field (g) and of the standard deviation of the distribution of the capillary pressure thresholds (W_t). The fragmentation process is not taken into account in this study. For an increase of g or/and when W_t decreases, two transitions are analyzed with three different regimes displacement patterns: Invasion percolation, invasion percolation in a gradient, and invasion in a pure gradient. The transitions are controlled both by the ratio g/W_t and by the sample size (L). A scaling law between the saturation at the percolation threshold and g/W_t allows delineating the three regimes in agreement with theoretical argument of the percolation in a gradient.

PACS. 47.55.Mh Flows through porous media – 61.43.Hv Fractals; macroscopic aggregates (including diffusion-limited aggregates) – 47.55.Kf Particle-laden flows

Introduction

The study of immiscible flow in a random porous media has been a very active area of research in the past and in recent years, in particularly due to its close connection with petroleum engineering and hydrology [1]. Particularly, the modeling of oil secondary migration [2] and non aqueous phase liquid migration in groundwater [3] is a major challenge due to the multi scale heterogeneous nature of the porous media [4]. The different physical and hydrodynamic parameters influencing the fluids flow are the gravity, the viscosity, and the capillarity. These forces can act simultaneously and have important implications in the determination of the non wetting fluid volume lost during migration.

In the absence of gravity and viscous effects, Invasion Percolation (IP) model has been used to simulate the slow displacement of a wetting fluid by a non wetting fluid in a porous medium [5,6]. The displacement is quasistatic and the process is represented by a cluster growth on a lattice of throats. The non wetting fluid enters preferentially in the larger throats where the capillary resistance is the smallest. Then, the invasion can be controlled by a step by step procedure and the capillary forces which are randomly distributed. At breakthrough, the percolation cluster is fractal. In the absence of trapping, theoretical argument can be developed for the fractal dimension calculations [7], leading for two dimensional system to $D = 91/48 \approx 1.89$. When the trapping rule is applied, regions surrounded by the invading phase become disconnected, and experiments and simulations have reported that the fractal dimension is $D \approx 1.82$ [6]. When the wetting and non-wetting fluids have different densities, the hydrostatic pressure density gradient produced will either stabilize or destabilize the fluid displacement process (Invasion Percolation in a Gradient, IPG). Gravity-stabilized invasion percolation [8–11] has been studied both numerically and experimentally. In this case, an invasion front propagates randomly and leaves behind trapped regions. When the stabilizing field gradient is increased, the percolation is influenced by the hydrostatic pressure gradient and this competition produces a decrease of the front width. Gravity-unstabilized invasion percolation was also studied both numerically [12,13] and experimentally [14,15]. The displacement pattern is then dominated by a single branch, and the width of this branch decreases if the density gradient is increased. On length scales smaller that the width of the branch, the structure of invasion is fractal, with the same fractal dimension as in IP displacement. The power law relating the width of the blobs and the field gradient was confirmed through

[a] e-mail: loggia@univ-montp2.fr

numerical simulations [12] and three dimensional column experiences [14]. More recently, the fragmentation [14–17] of invasion percolation cluster was analysed: this phenomena can occur when high density contrast allows snap-off events that produces migration of disconnected fragments of the non wetting fluid. An equal fractal dimension was found between the fragments and the IP percolation cluster [16,17]. The fragmentation structures could described in terms of standard IP and IPG theories, and it was pointed out that further study should take into account the effect of more complex heterogeneities.

In this study, we wish to investigate numerically the effect of the Probability Distribution Function (PDF) of the pore throat in an IPG destabilized process, in the absence of fragmentation process (for simplification reason). Hirsch [18] presented numerical simulations for three dimensional IPG. Based on simulations for different pore throat PDF, empirical relations were proposed for the saturation at the percolation threshold. However, in the network, the thresholds are controlled by the capillary pressure, which varies as the inverse of the throat size. Then, the capillary pressure PDF is a more tractable controlling parameter to study IP or IPG. Then, the heterogeneity influence for IPG in a destabilizing gradient was usually investigated for different capillary pressure PDF as in [11–13,15,19,20]. The exponent of the power law mentioned above (relating the width of the blobs and the field gradient) was found independent of the PDF [12]. The heterogeneity effect on invasion percolation was studied with spatially correlated networks, taking the invasion thresholds with self affine distributions [19,20]. It was shown that in the presence of trapping, the cluster is fractal, and its fractal dimension increases with the spatial correlation of the threshold distribution. In the presence of gravitational forces, it was recently shown that the width of the capillary pressure PDF controls the width of the percolation clusters [13,15]. This finding was studied in details with self affine distributions of the thresholds. The theory presented in [15] was generalized with gravitational and viscous forces, and confirmed with two dimensional experiments for stable IPG displacements [11]. Also, the idea that the standard deviation of the capillary pressure PDF controls the size of the cluster was given in a IP study with viscous forces and uniform distribution of threshold [21].

In the present article, we are interested in the non wetting residual loss during IPG in a destabilizing gradient. We use the same numerical method originally introduced in the study of the density gradient effect [12], and we analyse here the effect of the pore throat distribution which is related to the capillary pressure distribution. The fragmentation process is not considered.

We present the transitions occurring for a variation of the gradient field or/and the width of the capillary pressure PDF. Three main regimes are observed: IP, IPG, and purely vertical displacement. A subsequently analysis is then presented for the residual saturation and the transitions obtained.

Simulation

The simulations are performed using a step by step invasion percolation algorithm described in [8,12]. The porous medium is represented as a two-dimensional square network of wide throat of size $L \times L = 200 \times 200$. A lighter fluid displaces a denser fluid from the bottom to the top, in the presence of density and capillary forces. The density difference between the two fluids is noted $\Delta\rho$ and is taken positive. The gravity acceleration constant is noted g. As the displacement is considered slow and quasi-static, the viscous forces are neglected. As in [12], the trapping effect is taken into account, and we use periodic boundary conditions. The capillary pressure P_c is related to the pore throat r and the surface tension γ by means of the Laplace equation $P_c = 2\ \gamma/r$. The values of P_c are uniformly distributed over the range $P_c^{max} > P_c > P_c^{min}$. In the displacement of the non wetting fluid, the buoyancy force is opposed to the capillary pressure. For a pore located at a height h from the inlet, the invasion percolation algorithm is accomplished at each step where the difference pressure threshold

$$\Delta\rho\ g\ h - P_c \tag{1}$$

is maximum.

Theory

The flow is characterized by the dimensionless Bond number [8], $\mathrm{Bo} = \frac{\Delta\rho\ g\ \bar{r}^2}{\gamma}$ which is the ratio between gravitational and capillary pressure jump at the pore scale using the average pore throat size $\bar{r}$. In gravity-unstabilized percolation invasion, it was found that the displacement pattern is dominated by the growth of a single branch [12]. The width of this branch scales with the Bond number as $\xi_\perp \sim \mathrm{Bo}^{-\nu/(\nu+1)}$, where ν is the percolation exponent ($\nu = 4/3$ for the two dimensional system). It is important to note that for stable IPG process, this scaling law is again valid, but the characteristic length scale is parallel to the displacement [8,11,12]. Here, the displacement is unstable, and an increase of the Bond number enhances the instability and reduces the lateral width of the cluster $\xi_\perp$. For length scale smaller that $\xi_\perp$, the internal structure of the blobs is fractal, with a fractal dimensionality $D = 1.82$ in two dimension [12]. Thus, the cluster mass distribution verifies the relationship $M \sim \xi_\perp^D$, and the number of occupied sites by the invading fluid scales as $N \sim \xi_\perp^D\ \frac{L}{\xi_\perp}$. Then, at the scale of the whole network, the saturation of the invading fluid can be written as $S_0 \sim \frac{N}{L^2} \sim \frac{1}{L}\ \mathrm{Bo}^{-\alpha}$, with $\alpha = \frac{(D-1)\nu}{\nu+1}$. For two dimensional lattices, $\alpha \approx 0.47$, so the scaling law reads $S_0 \sim \mathrm{Bo}^{-0.47}$. Under the assumption that the distribution of the capillary pressure is slowly varying near the percolation thresholds [12,15], recent calculations have shown than the correlation length depends on the width of the capillary pressure PDF $W_t = P_c^{max} - P_c^{min}$ [13,15]. We wish to take into account the effect of W_t variations on So.

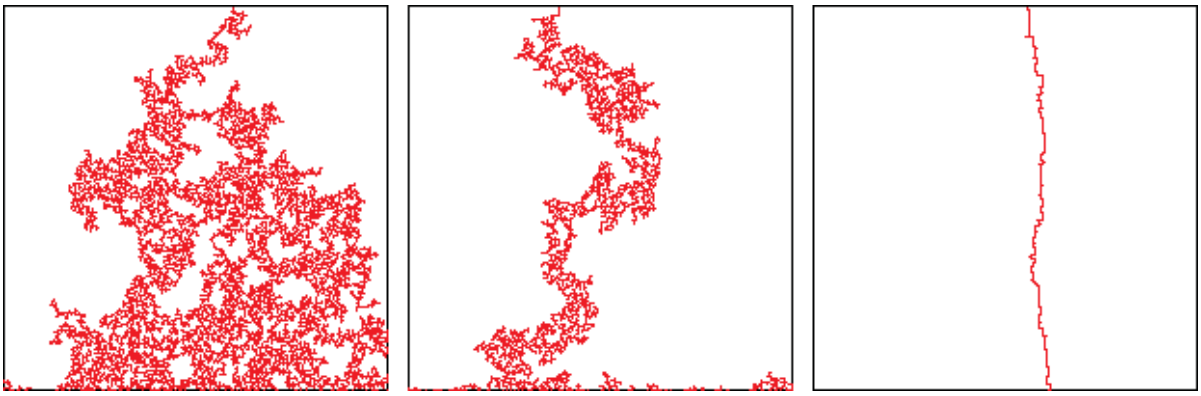

Fig. 1. Displacement patterns obtained from two dimensional gradient destabilized site invasion percolation simulations on a square lattice of size 200 × 200. Displacing fluid appears in black and is injected along the bottom edge of the lattice. The standard deviation of capillary pressure PDF is $W_t = 1$. From the left to the right: $\Delta\rho\ g$ are 0.05, 0.5, and 50.

The theory takes also into account the presence of viscous and gravitational forces [11]. As the viscous effects are neglected in our study, the result of references [11,13,15] can be written as $\frac{\xi}{r} \sim (\frac{\gamma}{W_t}\mathrm{Bo})^{-\alpha}$. Then, the preceding scaling law for the saturation reads

$$So \sim \frac{1}{L}\left(\frac{\gamma}{W_t}\mathrm{Bo}\right)^{-\alpha}. \qquad (2)$$

This result shows that the width of the capillary pressure distribution is an important parameter for the percolation properties in the IPG regime. It important to consider than this relation is not valid for all Bond number, because the fragmentation process should modify this scaling law. However, the transition from an IPG regime (or IP regime) to a fragmentation process is difficult to analyse quantitatively, because the transition is not only controlled by Bo. The fragmentation process can be enhanced by high density contrast (at high Bond number) or/and high height of non wetting fluid accumulation (not necessarily at high Bond number). This phenomena is then particularly complex, especially in the presence of heterogeneities, and it will not be considered here in first approach. Then in this paper, we use the results obtained from standard IPG simulation process, as introduced in [5], and intensive simulations are carried out to confirm equation (2) and to check its range of applicability for a large range of Bond number and a large range of width of the capillary pressure PDF.

Simulation results

An extensive series of simulations were carried out using the two-dimensional site-invasion gradient destabilized percolation model described above. In the simulation of Figure 1, the injection is done along the bottom edge of the lattice. However, the pattern rapidly evolves as a single branch; this effect is very noticeable for high Bond number. The images of Figure 1 show than the lateral width of the displacement pattern decreases with the Bond number. When Bo = 0, the process is only controlled by the pore throat size distribution (IP) [5,6], the string is not present and the invasion process is random. When the buoyancy forces increase, the probability for a vertical displacement increases with the density difference ($\Delta\rho$) and the height (h) of the connected cluster. This explains why the cluster width decreases with the Bond number [12]. For very high Bond number, the capillary forces are negligible, and the displacement pattern is dominated by a nearly vertical single branch (Fig. 1c). We call this regime Invasion in a Gradient (IG).

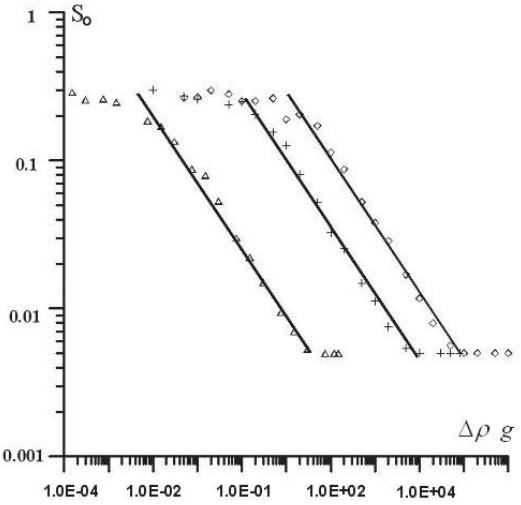

Fig. 2. So is plotted versus Bond number in a Log–Log plot for three fixed values of the width of the capillary pressure PDF ($W_t = 5\,\triangle$, and $W_t = 100\,+$, and $W_t = 1000\,\diamond$). The solid lines are a guide to the eye, with a –0.47 slope in accord with equation (2). Results are averaged over 1000 realizations.

The saturation at the percolation threshold is presented versus Bond number for four fixed values of W_t (Fig. 2). Simulations were performed using a bottom edge injection or a single point injection, but these boundaries conditions did not produce differences for all the results presented here. For the four values of W_t tested in this simulation, there are three domains in the curve. In the first one (for very low Bond number), the capillary forces dominate the displacement (IP), the saturation reaches a

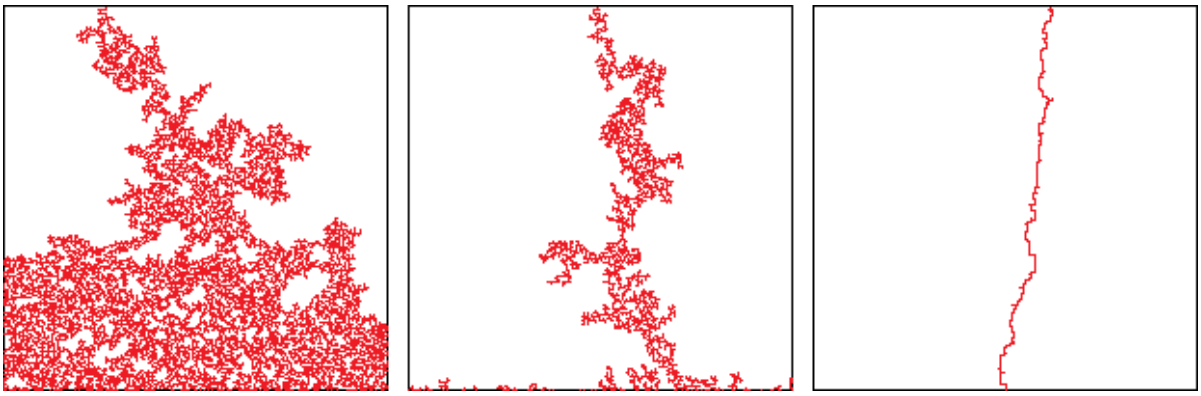

Fig. 3. Displacement patterns obtained from two dimensional IPG simulations on a square lattice of size 200×200. $\Delta\rho\ g = 0.2$ is now fixed, and we test the effect of the width of the capillary pressure PDF. From the left to the right W_t are 0.7, 0.1, and 0.02.

constant value. In the second domains, an increase of the density difference gives rise to a competition between capillary and buoyancy forces, and the power law between So and Bo is well verified (with $\alpha \approx 0.47$), in agreement with the theory of percolation in a destabilizing gradient [12]. In the third domains, for large Bond number, So reaches a second plateau. For infinite Bond number, the invading fluid pattern is a single and vertical line ($N = L$), so the asymptotical value for So at high Bond number is $1/L$. This behavior with three domains is very well verified for the four distributions of the capillary pressure. We observe than the transitions values from IP to IPG and IPG to IG do not occur for the same values of the Bond number, those transitions values depend on the width of the capillary pressure PDF. When the width of the capillary pressure PDF increases, the curve So of Figure 2 is shifted to the right. The pore throat size distribution is wider, and the effect of the density difference appears afterward with higher Bond number. This result suggests analyzing more precisely the effect of the capillary pressure PDF for a given value of the Bond number.

Simulations were carried out to investigate the effect of W_t. The typical resulting patterns of the displacement are presented in Figure 3, where $\Delta\rho\ g = 0.2$, and with three different tested values W_t. The figure reveals that the width of the cluster increases with the width of the capillary pressure PDF. For very large PDF, the high variability in the pore throat size distribution makes the resulting pattern very random. Although Bo $\neq 0$, the pattern is very similar to the pattern observed for very low Bond number (IP, Fig. 1a). In the other hand, for very narrow PDF, the capillary pressure threshold is less random, so the capillary pressure influence is hidden and the gravity forces predominate for this displacement: the structure of the cluster is nearly a single line as for very high Bond number (Fig. 1c). This transition from IP to IPG and to a string pattern when W_t decreases is similar to the previous transition described in Figure 1 when the Bond number increases. A more quantitative analysis of this transition is presented in Figure 4, where the saturation So at the percolation threshold is plotted versus $1/W_t$. As in Figure 2, the curve is divided in three parts: The first regime

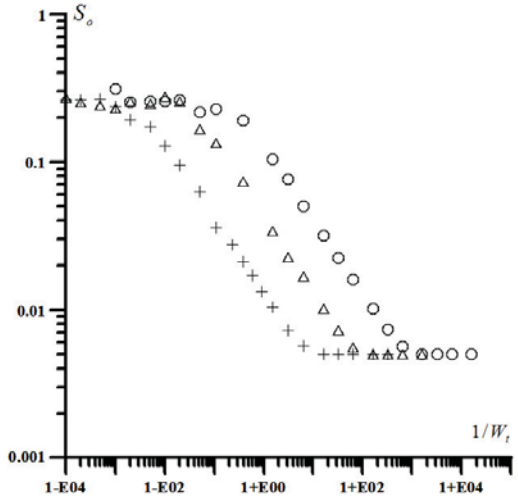

Fig. 4. So is plotted versus $1/W_t$ for three particular values of $\Delta\rho\ g$. ($\Delta\rho\ g = 20+$, $2\triangle$, and $0.2\circ$). Results are averaged over 1000 realizations.

corresponds to high values of W_t, where the saturation is nearly equal to 0.25 as in Figure 2 in the IP regime. In the second IPG regime, the power law So $\sim (1/W_t)^{-\alpha}$ is very well verified for all the tested values of the Bond number. These results are in good agreement with equation (2). As in Figure 2, we obtain the third IG regime, for low value of W_t, where the cluster becomes a single and nearly vertical line, with So $= 1/L$.

For a better understanding of the pore throat distribution influence, further simulations were carried out for different shape of the PDF of the capillary forces. Equation (1) was replaced by $\Delta\rho\ g\ h - \phi(P_c)$, where P_c is still a random number uniformly distributed over the range $P_c^{max} > P_c > P_c^{min}$, but ϕ is a non linear function which allows to change the PDF of the capillary pressure threshold. The results are shown in Figure 5, for $\Delta\rho\ g = 1$, and with 4 different functions ϕ. The scaling law for the So dependence on Bond number (Eq. 2) was numerically verified for different PDF in reference [12]. Here, we study the influence of $1/W_t$ on So. The power law (Eq. (2))

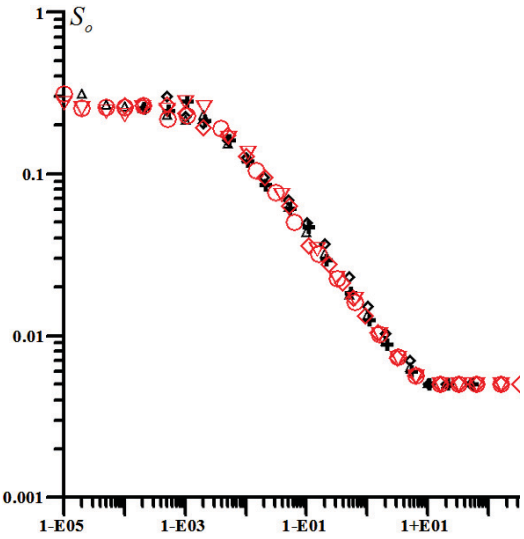

Fig. 5. Plot of the saturation So versus the rescaling variable Bo/W_t. All the datas of Figures 2 and 4 collapse on a single curve.

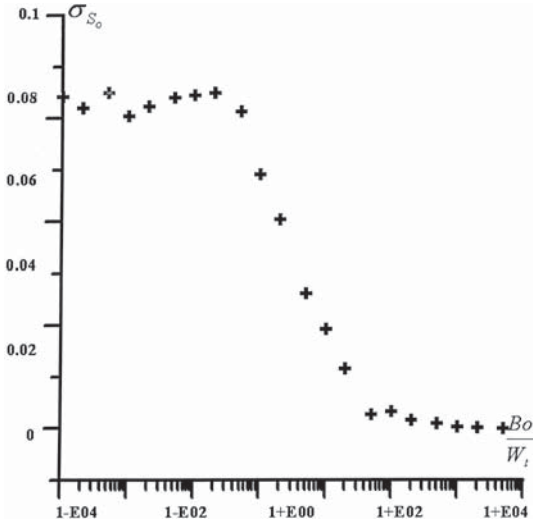

Fig. 6. Plot of the standard deviation of So versus the the rescaling variable Bo/W_t. σ_{So} is obtained using 1000 realizations on a 200×200 network. As in Figures 2, 4, and 5, the three regimes (IP, IPG, IG) can be distinguished.

is still valid whatever the PDF, with the same exponent $\alpha \approx 0.47$. This result can be explained using the same arguments as in [12,15]: at the first order and at the percolation threshold, all the PDF have the same shape near the invaded sites. This result demonstrates that it is correct to assume than the distribution of the capillary pressure is slowly varying near the percolation threshold [15]. So, the PDF does not affect the exponent of the power law. However, the amplitude of So is very sensitive to the PDF, it implies that the distribution and the magnitude of the capillary forces plays an important role in determining the displacement pattern and the saturation at the percolation threshold.

Discusion

The two transitions from IP to IPG and from IPG to IG are observed when Bo or/and $1/W_t$ increases. The control parameter is $\gamma \mathrm{Bo}/W_t$, this is a consequence of equation (2). This parameter was called the *the fluctuation number* in [11,15]. If we plot the results of Figures 2 and 4 versus the ratio γ Bo/W_t, all the points collapse on a single curve (Fig. 5). This curve validates equation (2). Also, it indicates than the capillary pressure distribution and the gravity field are both first order parameters for an accurate description of the IPG regime. Then, the fluctuation number is a much more suitable parameter than the Bond number [15]. It is important to precise that the validation of equation (2) requires averaging the results over different realizations, especially in the IP regime, where the disorder effect is more important. The behaviour of the standard deviation of So was studied versus Bo/W_t on a 200×200 network, and is shown in Figure 6. Each point of the standard deviation curve was obtained using 1000 realizations. As in Figures 2 and 4, there are again three domains in the curve. In the IP regime, σ_{So} is nearly constant. σ_{So} decreases in the IPG regime, but the decrease begins at $\mathrm{Bo}/W_t \sim 10^{-2}$, after the transition zone between the IP domain and IPG domain (observed at $\mathrm{Bo}/W_t \sim 10^{-3}$ in the Fig. 5). When $\mathrm{Bo}/W_t \geq 10$, the IG regime is reached, the branch is vertical and very narrow, and σ_{So} reaches asymptotically zero.

For a given value of W_t, the process at $\mathrm{Bo} = 0$ was studied in details in the past [5,6]. In this regime, the oil saturation at the percolation threshold scales as L^{D-2}, in relation with the fractal structure of the cluster at the percolation threshold. According to [12], when Bo increases, the capillary and gravity forces are then comparable, and the growth of a single branch will dominate the displacement pattern. The power law existing between So and Bo/W_t allows defining a scaling law for the threshold Bond number $\mathrm{Bo}^{IP-IPG} \sim W_t \; L^{-\frac{1+\nu}{\nu}}$, which is the critical Bo value for the transition from IP to IPG. This transition value is then directly proportional to W_t, so the capillary distribution controls significantly the transition described here. It is interesting to note that this transition value decreases with the size L of the system, because wider capillary pressure distribution or/and smaller network enhance random invasion process. This finding can be explained considering IPG branches of Figures 1 and 3: on a scale length smaller than the width of the branches, the structure of invasion is fractal as in IP displacements. Then, a a decrease of the length scale produces the transition from IPG to IP. Using similar argument, it is easy to precise the transition Bond number from IPG to IG, because the transition occurs when So reaches the asymptotic value $1/L$. The Bond number transition value scales simply as $\mathrm{Bo}^{IPG-IG} \sim W_t$. Then, if the width of the capillary pressure PDF increases, the curve in Figure 2 is shifted to the right. Finally, a similar analysis can be proposed to interpret Figures 4 and 5, when W_t is a variable with constant values of Bo. The values of W_t for the transitions from IP

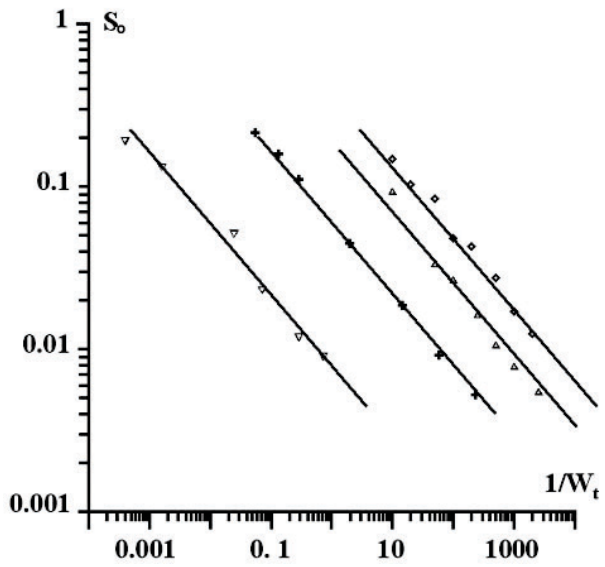

Fig. 7. So is plotted versus $1/W_t$ for different PDF shape of the capillary pressure (Gaussian $+$, x^2 ∇, uniform $\diamond$, $1/x$ $\triangle$), and $\Delta\rho\, g = 1$.

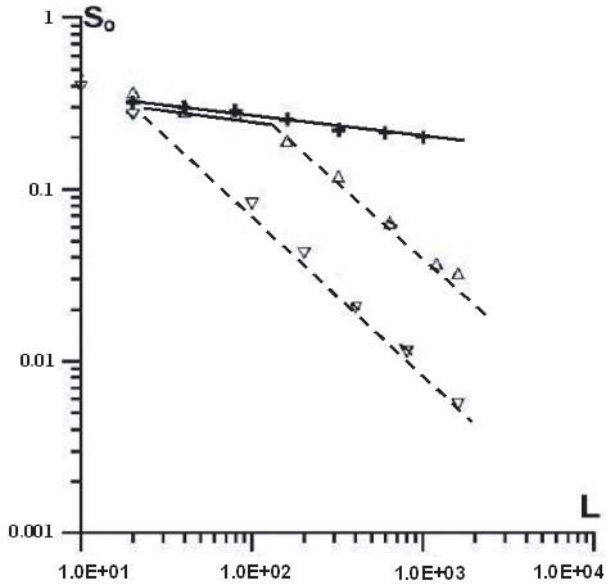

Fig. 8. So is plotted versus the size L of the $L \times L$ network, and for three density contrast: $\Delta\rho\, g$ are $0+$, $0.002\,\triangle$, and $0.04\,\nabla$. The lines are a guide to the eye. The slope of the solid line is -0.17, the slope of the dashed line is -1. Three regimes can again be distinguished: IP and IG (behaviour without cross over lengths) and IPG (behaviour with a cross over length between IP and IG).

to IPG and IPG to IG scale as $W_t^{IP-IPG} \sim \mathrm{Bo}\ L^{-\frac{\nu}{1+\nu}}$ and $W_t^{IPG-IG} \sim \mathrm{Bo}$ respectively.

Finally, the size of the system is an important parameter controlling the pattern and the saturation values at the percolation threshold. It also controls the transitions values (from IP to IPG). Indeed, the network size influence has to be analyzed in relation with the correlation length of the percolation cluster. For this reason, simulations were performed on system of various sizes, in order to check the transition between the different regimes, and the size dependence of the final saturation So. The results are presented in Figure 8, for the same capillary pressure distribution, but for three typical density contrasts. When $\mathrm{Bo} = 0$, the power law predicted by the percolation IP theory is $\mathrm{So} \sim L^{D-2}$. With two dimensional network, this last relation reads $\mathrm{So} \sim L^{-0.17}$, and is well verified in Figure 8, where the slope of the solid line is in good agreement with IP simulation results. For infinite Bond number, in the IG regime, the displacement is only vertical and the dependence of So on L is more important with $\mathrm{So} \sim L^{-1}$ (this is the dashed line of the Fig. 8). And in the intermediate IPG regime, the length over which the system is fractal divides the So relationship in two parts ($\mathrm{So} \sim L^{D-2}$ when $L \ll \xi_\perp$, and $\mathrm{So} \sim L^{-1}$ when $L \gg \xi_\perp$). It is important to note that the cross over length varies as a power law of the fluctuation number as $(\frac{\gamma}{W_t}\mathrm{Bo})^{-\alpha}$. For a fixed network size, an increase of the fluctuation number will reveal the two transitions from IP to IPG, and IPG to IG (Figs. 1 and 3). For a fixed fluctuation number and a varying size system, the situation is a little more complex: Transitions from IP to IPG (respectively from IPG to IP) are possible when the network size increases (respectively decreases). However, the IG regime is not affected by the network size, because a vertical string remains identical at all the scales. All these different scaling laws have important implications for a better understanding of the non wetting residual loss.

Conclusion

For quasistatic invasion controlled by capillary forces under a destabilizing gradient, the displacement patterns are controlled both by the Bond number, the width of the capillary pressure PDF, and the size of the system. When $\frac{\gamma\,\mathrm{Bo}}{W_t} \ll L^{-\frac{1+\nu}{\nu}}$, the behavior of the non wetting cluster is same as in invasion percolation. When $1 \gg \frac{\gamma\,\mathrm{Bo}}{W_t} \gg L^{-\frac{1+\nu}{\nu}}$, the gravity and the capillarity act simultaneously, and this regime is characterized by the growth of a single branch (invasion percolation in a gradient). When $\frac{\gamma\,\mathrm{Bo}}{W_t} \gg 1$, the gravity effect predominates and hides the heterogeneity and the capillary forces; the displacement is then purely vertical (invasion in a gradient). The different regimes are controlled both by the gravity and the heterogeneity field through the fluctuation number $\gamma\ \mathrm{Bo}/W_t$. It important to underline than the scaling law found here are only applicable in the absence of fragmentation process. However, the model reveals important quantitative aspects of vertical non wetting fluid displacement, and it may provide a basis for further studies. The present model uses spatially uncorrelated capillary pressure distribution. Further investigations are needed with more complex heterogeneities. The presence of viscous forces should also be considered.

This work is supported by the Chinese national 973 Project No. G199904310 and the French embassy in China.

References

1. F.A.L. Dullien, *Porous Media Fluid Transport and Pore Structure*, 2nd edn. (Academic, San Diego, 1992)
2. A.D. Hindle, AAPG Bulletin, **81**, 1451 (1997)
3. C.W. Fetter, *Contaminant Hydrogeology* (Macmillam Publishing Company, New York 1992)
4. M. Sahimi, Rev. Mod. Phys. **65**, 1393 (1993)
5. D. Wilkinson, J.F. Willemsen, J. Phys. A **16**, 3365 (1983)
6. R. Lenormand, C. Zarcone, Phys. Rev. Lett. **54**, 2226 (1985)
7. J. Feders, *Fractals* (Plenum, New York 1988)
8. D. Wilkinson, Phys. Rev. A. **30**, 520 (1984)
9. D. Wilkinson, Phys. Rev. A **34**, 1380 (1986)
10. A. Birovljev, L. Furuberg, J. Feder, T. Jøssang, K.J. Måløy, A. Aharony, Phys. Rev. Lett. **67**, 584 (1991)
11. Y. Méheust, G. Løvoll, K.J. Måløy, J. Schmittbuhl, Phys. Rev. E **66**, 051603 (2002)
12. P. Meakin, J. Feder, V. Frette, T. Jøssang, Phys. Rev. A. **46**, 3357 (1992)
13. J. Schmittbuhl, A. Hansen, H. Auradou, K.J. Måløy, Phys. Rev. E **61**, 3985 (2000)
14. V. Frette, J. Feder, T. Jøssang, P. Meakin, Phys. Rev. Lett. **68**, 3164 (1992)
15. H. Auradou, K.J. Måløy, J. Schmittbuhl, A. Hansen, D. Bideau, Phys. Rev. E **60**, 7224 (1999)
16. G. Wagner, P. Meakin, J. Feder, T. Jøssang, Physica A **245**, 217 (1997)
17. G. Wagner, A. Birovljev, P. Meakin, J. Feder, T. Jøssang, Phys. Rev. E **55**, 7015 (1997)
18. L. M. Hirsch, A. Thompson, Phys. Rev. B **50**, 2069 (1994)
19. L. Paterson, S. Painter, M.A. Knackstedt, W.V. Pinczewski, Physica A **233**, 619 (1996)
20. G. Wagner, P. Meakin, J. Feder, T. Jøssang, Phys. Rev. Lett. **55**, 1698 (1997)
21. B. Xu, Y.C. Yortsos, D. Salin, Phys. Rev. E **57**, 739 (1998)